PHARMACIA

Pharmacia 71: 1–14
DOI 10.3897/pharmacia.71.e118323

Research Article

Design and optimization of pantoprazole sodium mucoadhesive hydrogel microcapsules for the healing of peptic ulcers

Rashad M. Kaoud[1], Mustafa Hasan Alwan[1], Mohammed Amran[2], Hayder Adnan Fawzi[3]

1 *College of Pharmacy, Ashur University, Baghdad, Iraq*
2 *Department of Pharmacy, Al-Manara College for Medical Sciences, Maysan, Iraq*
3 *Department of Pharmacy, Al-Mustafa University College, Baghdad, Iraq*

Corresponding author: Hayder Adnan Fawzi (haider-pharm@almustafauniversity.edu.iq)

Received 5 January 2024 ♦ **Accepted** 21 April 2024 ♦ **Published** 18 July 2024

Citation: Kaoud RM, Alwan MH, Amran M, Fawzi HA (2024) Design and optimization of pantoprazole sodium mucoadhesive hydrogel microcapsules for the healing of peptic ulcers. Pharmacia 71: 1–14. https://doi.org/10.3897/pharmacia.71.e118323

Abstract

Hydrogels have gained much focus as a gastro-retentive technology for drug delivery. The current study aimed to design an oral mucoadhesive sustained-release dosage form to lower peptic ulcer complications (PUC). Using the Box-Behnken statistical design, the preparation method was developed by incorporating pantoprazole sodium (PZS) into hydrogel microcapsules (HGMC). The PZS was incorporated into the HGMC via an ion gelation technique, with sodium alginate as the gelling agent, calcium chloride as the crosslinking agent, and chitosan as the agent for sustained release.

The optimized formulation of PZS-HGMC showed a diameter of 2.506 mm, a swelling rate of 838.2%, and an encapsulation efficiency of 93.8%. Scanning electron microscopy images revealed the microcapsules' spherical shape. The in vitro release of the PZS from the HGMC after two hours in a simulated gastric fluid was 13.2%1±0.08%, compared with the apparent solubility of the pure PZS under the same conditions (95.24%±3.2%). After 24 hours, the percent of PZS released from the optimized formula was 69.84±2.4%, which indicates a sustained release pattern. The results from the in vivo study demonstrated improved healing of the induced ulcers in rats when treated with the PZS-HGMC formulation as compared to the standard PZS therapy; therefore, the obtained mucoadhesive HGMC was considered a potential drug delivery strategy for PUC therapy.

Keywords

anti-ulcerogenic effect, Box-Behnken design, histopathological analysis, in vitro release

Introduction

A peptic ulcer is defined as a disruption in the mucosal lining of the gastrointestinal system, specifically in the stomach and upper part of the small intestine, caused by the release of acid or pepsin (Lanas and Chan 2017). Moreover, peptic ulceration penetrates the mucosa section, causing mucosal lesions and leading to digestive tract inflammation (Najm 2011; Lanas and Chan 2017). The management of peptic ulcers involves alleviating pain, promoting ulcer recovery, and averting potential sequels (Yuan et al. 2006). The availability of histamine (H2)-receptor antagonists and proton pump inhibitors (PPIs) broadens the treatment options for peptic ulcers (Yuan et al. 2006). Peptic ulcer complications (PUC) are usually treated with proton pump inhibitors (PPIs) over long periods of time (Khan and Howden 2018).

Pantoprazole sodium (PZS) is an effective PPI; it acts by irreversibly binding the parietal cells' proton pump, which will hinder the main source of acid production in the stomach (Yu et al. 2017). PZS is a powerful tool when treating PUC and reflux esophagitis. Because PZS inhibits the hepatic microsomal P-450 monooxygenase pathway, medicines metabolized by this enzyme may acquire a longer serum half-life on simultaneous intake (Shin and Sachs 2008).

PZS possesses excellent permeability, solubility, and absolute bioavailability (77%) (Pue et al. 1993), oral bioavailability (80%–85%) (Pue et al. 1993), and a half-life of 1.0 hour. In addition, it can be given both orally and intravenously (Joseph et al. 2015). PZS is quickly absorbed and strongly protein-bound (98%). Maximal absorption occurs 2.5 hours after a single or multiple oral delivery (Joseph et al. 2015). Due to a rise in drug absorption when intragastric acidity lowers, the bioavailability of PZS rises with repeated doses up to around four days (Bigoniya et al. 2011).

Currently, PZS is available in such standard-approved formulations as tablets (EC polymer: methacrylic acid-ethyl acrylate copolymer (1:1) and controloc control), oral suspension (granules, enteric-coated polymer (methacrylic acid copolymer), and powder for solutions for injections (such as sodium hydroxide) (Srebro et al. 2022). In addition, other formulations still lacking official approval are the nanoprecipitation method (Nasef et al. 2017; Sheikh and Asati 2022), microparticles (Comoglu et al. 2008; Raffin et al. 2008; Dhurke et al. 2013; Raj et al. 2015; Hamzah and Kassab 2024), enteric-coated minitablets (Szczepanska and Sznitowska 2019), enteric-coated pellets (Han et al. 2018), sustained release floating tablets (Reddy et al. 2018), hydrogel (Gupta and Shivakumar 2009; Taher et al. 2018; Sudhakaran et al. 2021), and the sustained release mucoadhesive gastroretentive system (Reddy and Jalajakshi 2018). These formulations were developed to address the various issues with the oral administration of this drug, including premature activation in the stomach since its absorption occurs in the duodenum (Shin and Sachs 2008) and increasing its duration of action (Srebro et al. 2022).

PUC can be treated in several ways, including using mucoadhesive HGMC drug delivery systems. HGMC have been studied as a potential gastroprotective dosage form because of their capacity to increase the bioavailability of PZS when taken orally by serving as a sustained-release dosage form (Gadge et al. 2019).

This study aims to formulate an oral mucoadhesive sustained-release dosage form containing pantoprazole sodium hydrogel microcapsules (PZS-HGMC) using the Box-Behnken design and then undergo characterization studies, an in vivo study (including histopathological examination), and an in vitro release study for the optimized PZS-HGMG formula.

Materials and methods

Materials

Pantoprazole sodium, sodium alginate, and chitosan were gifted by Al-Hikma Pharmaceuticals (Cairo, Egypt). Hydrochloric acid (HCl) and calcium chloride (anhydrous fine GRG 90%) were purchased from the Al-Nasr Company for Pharmaceuticals (Cairo, Egypt). Generally, all the chemicals used were of analytical grade.

Optimization of formulation variables

The Box-Behnken statistical design with three factors, three levels, and 15 runs was chosen for the optimization analysis. Theoretically, the experimental design consists of points at the midpoint of each edge and the replicated center point of the multi-dimensional cube.

The dependent and independent variables in the experimental design of the microcapsules (MC) formulated by sodium alginate (SAT) and coated with chitosan (CTN) are presented in Table 1. Using the software Design Expert® (Version 7.0.0, Stat-Ease Inc., Minneapolis, MN, USA) and Minitab® 17.1.0, the following equation (quadratic model) was applied for designing the different formulas:

$$Yo = b_0 + b_1X_1 + b_2X_2 + b_3X_3 + b_{12}X_1X_2 + b_{13}X_1X_3 + b_{23}X_2X_3 b_{11}X_{21} + b_{22}X_{22} + b_{33}X_{23}$$

Y0 is the dependent variable; b0 is an intercept; b1 to b33 are regression coefficients computed from the observed experimental values of Y; and X1, X2, and X3 are the coded levels of independent variables. X1X2 and Xi2 (i = 1, 2, or 3) represent the interaction and quadratic terms, respectively.

The primary constituents of the PZS-HGMG include PZS (20 mg), SAT, CTN, and calcium chloride ($CaCl_2$). These choices were made based on the initial experiments for the formulation of PZS-HGMG. The experimental design investigated the connection between the independent variables and their responses and interactions in an effective model. It involved three variables and three responses. While the independent variables were the concentration of SAT (X1), the concentration of $CaCl_2$ (X2), and the concentration of CTN (X3), the measured dependent variables were particle diameter (Y1), swelling degree (Y2), and encapsulation efficiency (Y3), as represented in Table 1.

Table 1. Independent and dependent variables applied in a Box-Behnken design.

Factors	Independent variables		Low (-1)	Medium (0)	High (+1)
X_1	Sodium Alginate (SAT)	%	1	2	3
X_2	Calcium Chloride ($CaCl_2$)	%	2	3	4
X_3	Chitosan (CTN)	%	0.1	0.3	0.5
Response					
Y_1	Particle Diameter	mm			
Y_2	Swelling (SW%)	%			
Y_3	Encapsulation Efficiency (EE%)	%			

Preparation of PZS-HGMG

The pantoprazole-loaded hydrogel microcapsules of alginate core and chitosan coating were prepared using the ion gelation method with some modifications (Ramos et al. 2018; Karakas et al. 2022; Padhmavathi et al. 2023).

As a first stage of formulation, SAT (1%–3% w/v) was dissolved in deionized water (20 mL) and stirred (900 rpm) at 25 °C. Then PZS 20 mg was dissolved in deionized water (10 mL) as the first solution. The second solution consisted of CTN (0.1%–0.5%) and CaCl2 (2%–4%) dissolved in a 1% v/v acetic acid solution, which was used as a coagulation fluid. The first solution was molded into a second homogenous solution with 0.1 N HCl, and the pH was adjusted to 5±0.1. A 1 mL/min pumping rate was used to keep the combined flow constant. After being stirred in the fluid for 20 minutes, PZS-HGMG was formulated. The PZS-HGMG were filtered, washed, and dried at 25±0.5 °C (Gioumouxouzis et al. 2018; Rostami 2020).

Optimization employing Box-Behnken design

The optimized formula was chosen according to the response to the desirability of variables (by maximizing particle diameter, swelling, and encapsulation efficiency). Physicochemical, in vitro, and in vivo analyses were conducted for the optimized formula.

It was validated statistically by constructing quadratic equations for the diameter of the response, SW% studies, and the EE% (Y1, Y2, and Y3), respectively.

Characteristics of the PZS-HGMG

Microcapsule diameter analysis

The PZS-HGMC were measured for diameter with a micrometer screw gauge, and the mean was then calculated (Zeeb et al. 2015).

Swelling experiments (SW%)

The SW% of the HGMC was investigated via the immersing method (Anal and Stevens 2005) in detail. The SW study was conducted in a water bath shaker at 37±0.5 °C. Previously weighted HGMC were immersed in 0.1N HCl for two hours, resulting in the HGMC swelling. The swollen HGMC were wiped with filter paper to eliminate excessive buffer and then weighed. All significant shifts in weight were recorded. The SW% was calculated by the following formula (Taher et al. 2019):

$$SW\% = \frac{\text{Weight of swollen MCs} - \text{Weight of dry MCs}}{\text{Weight of dry MCs}} \times 100$$

Encapsulation efficiency (EE%)

The drug content of the PZS-HGMG was directly measured. The PZS-HGMG (200 mg) was carefully weighed and crushed. The PZS-HGMG were mixed with deionized water (10 mL) for a full day at 25±0.5 °C. Then, the solution was filtered through a nano-filter syringe. The PZS concentration was detected spectrophotometrically using the UV-visible spectrophotometer (Shimadzu, Japan) at 283 nm. The EE% was detected using the following equation (Umaredkar et al. 2020):

$$(\%EE) = \frac{RA}{TA} \times 100$$

RA and *TA* are the resulting and theoretical amounts of PZS found in the PZS-HGMG, respectively. The results were repeated in triplicate.

SEM analysis

The morphologies and surface of the PZS-HGMG were investigated using SEM (Agilant 8500 FE, Japan) (Thanos et al. 2006). PZS-HGMG samples were covered with gold and photographed at a voltage of 30 kV before being placed on aluminum stubs for examination.

FTIR analysis for an optimized formula

Before submitting samples for FTIR evaluation, a pestle and mortar were used to reduce the PZS-HGMG to a powder. The FTIR probe examined the sample (JASCO FTIR Model 6600, Tokyo, Japan). The range was selected from 400 to 4000 cm^{-1} with 95% transmittance. Interactions can be detected, and functional group alterations can be identified using FTIR spectral analysis (FTIR spectrophotometer at a scanning number of 8 with the KBr sampling method) (Moghaddam et al. 2015).

DSC studies for an optimized formula

Some differential scanning calorimetry (DSC) studies were applied using DSC 60 TASYS Software (Shimadzu, Japan). The dry MCs used in the DSC trial varied from 3 to 7 mg. The sample was analyzed in a nitrogen flow with a 25–300 °C temperature, and the scan rate was 10 °C/min. The DSC detects crystallinity changes, melting points, and drug-excipient-adsorbent interactions (Honary et al. 2009).

In vitro drug release

The PZS release experiment used a USP apparatus type II (Copaly, United Kingdom) at 100 rpm and 37 °C. Then 20 mg of PZS-HGMG and PURE PZS were placed in hard gelatin capsules, and then the capsules were placed in 0.1N HCl (pH 1.2) to simulate the stomach environment over 24 hours. At each of the 24-hour intervals (10 intervals), 5 mL aliquots were removed and refilled with fresh dissolution media. The PZS concentration of each sample was determined at 283 nm spectrophotometrically (Shimadzu, Japan). The test was conducted in triplicate (Heikal et al. 2023).

In vivo anti-ulcerogenic study

The in vivo study was prepared following the ARRIVE Guidelines 2.0. Male Wistar rats (weighted around 180–200 g and ages 3–5 months) were received from the animal facility in the Pharmacy Department at Ashur University College. They were maintained at 25 °C and a light/dark cycle (12 hours light and 12 hours dark). The animals received commercial pellet feed and had free access to water. They were acclimated for 10 days before starting the experiment at the same center where the rats were obtained.

For sample size computation, the program G Power was utilized (Faul et al. 2007) based on Cohen's principles

(Charan and Kantharia 2013). The groupings were constructed randomly using a table of random integers. The mice were systematically allocated into properly marked boxes and individually identified with tail tags to mitigate the occurrence of misinterpretation (Festing 2006).

The study modules employed a randomized block design. The mice were categorized into five distinct blocks. Block one (G1) received their treatment plan. Then, in order in subsequent weeks, Block two (G2), Block three (G3), Block four (G4), and Block five (G5) commenced their respective treatments. Details of the animal allocation and drug dosing are illustrated in Table 2.

Table 2. Animal allocation for each group.

	Indomethacin[a]	Drug received (eight weeks)	Duration
G1	Did not receive	normal saline by gastric gavage	15 days
G2 (Bhattacharya et al. 2007; Sabiu et al. 2015)	Received	normal saline by gastric gavage	15 days
G3	Received	blank HGMC by gastric gavage	15 days
G4 (Xie et al. 2005)	Received	PZS pure (20 mg/kg) by gastric gavage	15 days
G5 (Xie et al. 2005)	Received	PZS-HGMC optimized formula (20 mg/kg) by gastric gavage	15 days

[a] Indomethacin: single dose of 30 mg/kg/day of IMN orally by gastric gavage. Each set was conducted in triplicate.

Induction of ulcers by indomethacin (IMN) was done (induction of gastric ulcers was done following previous studies) (Bhattacharya et al. 2007; Sabiu et al. 2015). The rats were given a single oral dose of IMN 1% sodium carboxymethylcellulose (CMC) (30 mg/kg body weight as a 2 ml solution), then they fasted for 24 hours, but they were allowed free access to water during this period.

In each group, the rats received the optimized formula once per day for 15 days. On the 16th day, all animals had a period of fasting lasting 10 hours. Subsequently, they were subjected to intraperitoneal (IP) anesthesia with a dosage of 80 mg/kg of ketamine (Ketamine 10%, Alfasan Nederland BV, Holand) and 10 mg/kg of xylazine (XYL-M2, VMD® Livestock Pharma, Belgium). After undergoing complete anesthesia, the rats were euthanized using carbon dioxide (Underwood and Anthony 2020; Yaribeygi et al. 2023).

The stomachs of the rats were extracted and macroscopically evaluated for bleeding ulcers. The number and intensity of lesions per piece of gastric tissue were recorded microscopically. Lesions were assessed visually after opening the stomach, cleansing with ice-cold saline, and coating with filter paper (El-Deen et al. 2016).

Histological assessment of rats' gastric tissues

The pieces of gastric tissue were preserved by immersion in 10% formalin and subsequent fixation in paraffin. Pieces of 5–6 µm thickness were colored with hematoxylin and eosin. The Sydney system was applied to assess microscopic changes in the gastric mucosa, including chronic lesions, dropout gland (atrophy) regions, and intestinal metaplasia (Dixon et al. 1996).

Ethical approval

Following CPCSEA regulations, the Institutional Animal Ethics Committee authorized the experimental protocols for research project number RP62 (date: 2 December 2022).

Statistical analysis

Experimental results are the mean±standard deviation (SD). The significance of differences was tested by analyzing variance (ANOVA). Differences were considered statistically significant at $P \leq 0.05$.

Results and discussion

Formulation and optimization using a Box-Behnken design

Realizing the complexity of producing pharmaceutical formulations is made easier by the numerous benefits and the adaptability of the design. Several independent parameters govern the number of experiments required, whereas the responses for every trial are established and the multiple regression analysis is performed.

The current study employs a straightforward design with just three independent variables across three distinct levels of experimentation. All batches of the formulations were made as planned and tested for various responses. Using ANOVA (Analysis of Variance), the present study investigated each variable alone and interacted with the other responses to improve the outcomes. Using Design Expert® software and an ANOVA analysis, it produced 15 different formulations. It validated them statistically by constructing quadratic equations for the diameter of the response, SW% studies, and the EE% (Y1, Y2, and Y3), respectively, as illustrated by Table 3. The Box-Behnken Design was used, and the results were analyzed and proved using a significant coefficient with R^2 values across the entire region of experimentation. In addition, optimum checkpoint formulations were generated and analyzed to determine the optimized formula for the given experimental domain and Box-Behnken design equations.

Diameter

The resulting PZS-HGMG had diameters ranging from 1.3 to 2.5 mm by vernier caliper (Gulia et al. 2023), as displayed in Table 3.

Swelling (%)

Table 3 illustrates the swelling behavior of the PZS-HGMG at pH 1.2; the obtained SW% ranges from 410.0% to 840.0%.

Table 3. Experimental design for the formulations of PZS-HG-MC using a Box-Behnken design.

Run	SAT (%)	$CaCl_2$ (%)	CTN (%)	SAT (%)	$CaCl_2$ (%)	CTN (%)	Diameter (mm)	Swelling (SW%)	(EE%)
F1	-1	-1	0	1.0	2.0	0.3	1.6±0.20	410.0±43.5	88.0±2.0
F2	1	-1	0	3.0	2.0	0.3	2.5±0.26	735.0±26.6	92.0±1.7
F3	-1	1	0	1.0	4.0	0.3	1.3±0.26	460.0±27.6	90.0±2.6
F4	1	1	0	3.0	4.0	0.3	2.5±0.10	800.0±30.0	93.0±1.0
F5	-1	0	-1	1.0	3.0	0.1	1.4±0.26	470.0±30.8	89.0±2.0
F6	1	0	-1	3.0	3.0	0.1	2.3±0.10	740.0±30.3	93.0±3.0
F7	-1	0	1	1.0	3.0	0.5	1.3±0.17	490.0±26.5	87.0±2.6
F8	1	0	1	3.0	3.0	0.5	2.3±0.20	840.0±55.0	94.0±3.0
F9	0	-1	-1	2.0	2.0	0.1	2.3±0.10	500.0±39.0	90.0±3.0
F10	0	1	-1	2.0	4.0	0.1	2.1±0.17	520.0±29.4	91.0±2.6
F11	0	-1	1	2.0	2.0	0.5	2.2±0.10	500.0±26.5	90.0±3.5
F12	0	1	1	2.0	4.0	0.5	2.2±0.10	520.0±27.9	91.0±2.6
F13	0	0	0	2.0	3.0	0.3	2.0±0.17	510.0±32.9	91.0±2.0
F14	0	0	0	2.0	3.0	0.3	2.0±0.20	510.0±26.5	91.0±2.6
F15	0	0	0	2.0	3.0	0.3	2.0±0.30	510.0±33.0	91.0±1.7

Data presented as mean±SD, n = 3.

The PZS-HGMG showed swelling, resulting in MC with a small amount of SAT bursting after two hours of testing. The Na^+ ion in the used buffer and the Ca^{2+} ion in the cavity of Ca-alginate microcapsules are involved in the ion exchange mechanism (Elnashar et al. 2010). One possible cause of swelling involves the exposure of the dry PZS-HGMG to water, and the hydrophilic SAT and CTN groups caused them to swell (Khan et al. 2023).

Drug encapsulation efficiency (EE%)

The EE% was 87.0 to 94.0%; the greater EE% of the SAT–CTN microcapsules may be attributed to the more porous structure (Dhurke et al. 2013). Since Ca^{+2} and $-NH_3^+$ of CTN compete, they can react with –COO– of SAT (Akyuz et al. 2017). The estimated values of EE are illustrated in Table 3.

Development of the optimized model

The optimized PZS-HGMG formula was developed using the indicated concentrations of variables from an overlay plot to ensure the model's accuracy. The effect of changing the concentrations of $CaCl_2$, SAT, and CTN on response parameters (PZ, SW%, and EE%) was examined. The desirability of the optimized formula in this experiment would have maximum EE%, SW%, and PZ in the range.

Particle size (PS)

By fixing the effects of one parameter, one can examine the effects of the other two parameters with PS; thus, by holding the CTN concentration constant, SAT has a direct relationship with PS, and $CaCl_2$ did not affect PS (Fig. 1A).

By holding the $CaCl_2$ concentration constant, PS appeared to be directly associated with SAT, while CTN did not affect PS (Fig. 1B).

By holding the SAT concentration constant, both CTN and $CaCl_2$ have a direct relationship with PS (Fig. 1C).

The overall adjusted R^2 of the model was 99.11%, with SAT showing 84.75% contribution of the final model (p-value < 0.001), with SAT (r = 0.5, p-value < 0.001), $CaCl_2$ (r = -0.0625, p-value = 0.006), SAT*SAT (r = -0.2, p-value < 0.001), $CaCl_2$*$CaCl_2$ (r = 0.175, p-value < 0.001),

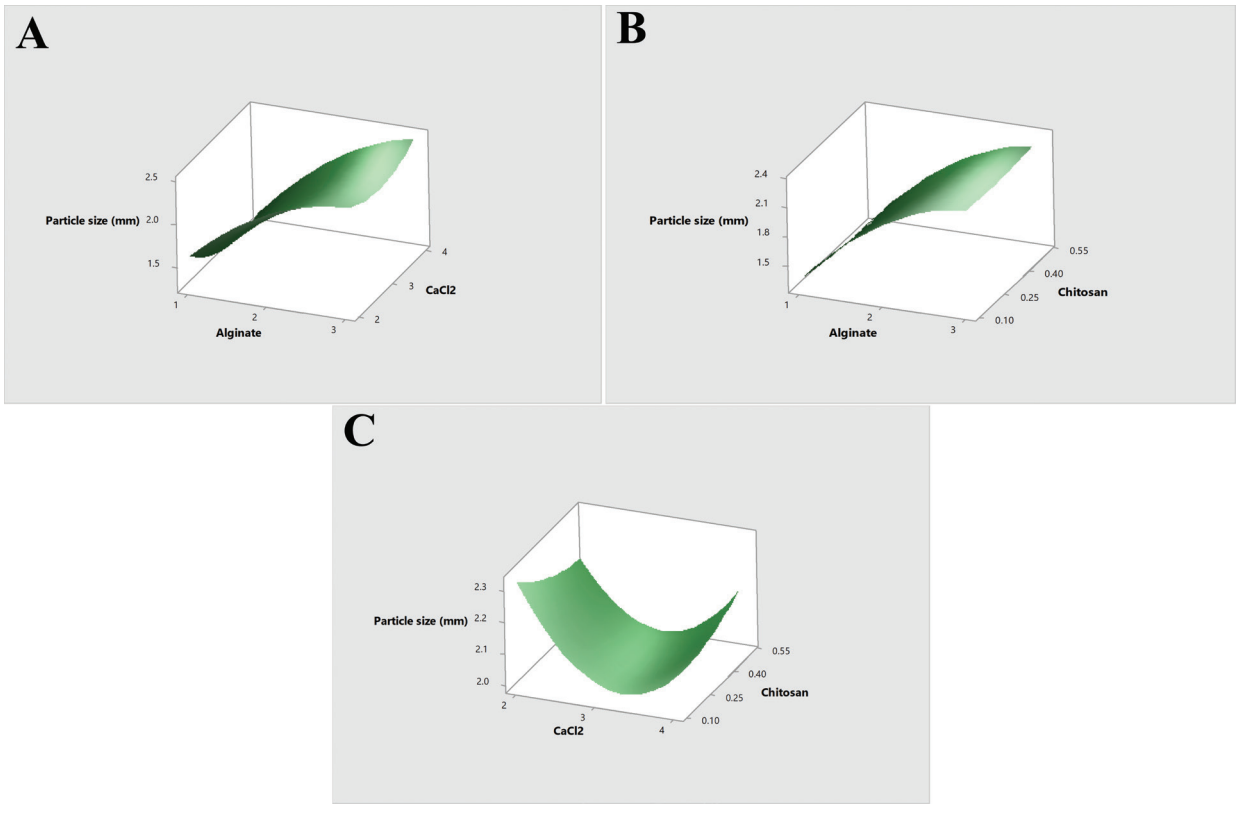

Figure 1. Response surface graphs show variables' effects on (**A, B, C**) particle size.

and SAT*$CaCl_2$ (r = 0.075, p-value = 0.012) are the significant coefficients in the final model:

Particle size (*mm*) = 2.787 + 1.038 *Alginate* – 1.338 *CaCl*2 – 1.437 *Chitosan* – 0.2000 *Alginate* * *Alginate* + 0.1750 *CaCl*2 * *CaCl*2 + 0.625 *Chitosan* * *Chitosan* + 0.0750 *Alginate* * *CaCl*2 + 0.1250 *Alginate* * *Chitosan* + 0.2500 *CaCl*2 * *Chitosan*

Swelling (%)

By fixing the effects of one parameter, one can examine the effects of the other two parameters with SW%; thus, by holding the CTN concentration constant, SAT has a direct relationship with SW%, and $CaCl_2$ did not affect SW% (Fig. 2A).

By holding the $CaCl_2$ concentration constant, SW% appeared directly associated with SAT, while CTN did not affect SW% (Fig. 2B).

By holding the concentration of SAT constant, both CTN and $CaCl_2$ have a direct relationship with SW% (Fig. 2C).

The overall adjusted R^2 of the model was 97.0%, with SAT showing a 78.92% contribution to the final model (p-value < 0.001), with SAT (r = 160.63, p-value < 0.001), and SAT*SAT (r = 108.1, p-value < 0.001) as the significant coefficients in the final model:

Swelling (%) = 509 – 313.1 *Alginate* + 113.1 *CaCl*2 – 378 *Chitosan* + 108.1 *Alginate* * *Alginate* – 16.9 *CaCl*2 * *CaCl*2 + 422 *Chitosan* * *Chitosan* + 3.8 *Alginate* * *CaCl*2 + 100.0 *Alginate* * *Chitosan* - 0.0 CaCl2 * *Chitosan*

Encapsulation efficacy (%) (EE%)

By fixing the effects of one parameter, one can examine the effects of the other two parameters with EE%. By holding the CTN concentration constant, SAT and $CaCl_2$ have a direct relationship with EE% (Fig. 3A).

Holding the $CaCl_2$ concentration constant, EE% appeared to be directly associated with SAT and CTN (Fig. 3B).

By holding the concentration of SAT constant, both CTN and $CaCl_2$ have a direct relationship with EE% (Fig. 3C).

The overall adjusted R^2 of the model was 87.13%, with SAT showing an 82.77% contribution to the final model (p-value < 0.001), with SAT (r = 2.25, p-value < 0.001), and $CaCl_2$ (r = 0.625, p-value = 0.046) as the significant coefficients in the final model:

Encapsulation efficacy (%) = 82.75 + 1.88 *Alginate* + 2.62 *CaCl*2 – 4.38 *Chitosan* – 0.000 *Alginate* * *Alginate* – 0.250 *CaCl*2 * *CaCl*2 – 6.25 *Chitosan* * *Chitosan* – 0.250 *Alginate* * *CaCl*2 + 3.75 *Alginate* * *Chitosan* + 0.00 *CaCl*2 * *Chitosan*

Effect of SAT

The concentration of SAT increased, and the diameter increased (Fig. 1A, B). This result is compatible with the outcomes of (Patil et al. 2012). The model graphs indicated that SAT significantly impacts the SW of various formulations (Fig. 2A, B). When the content of SAT grew, the formulations swelled, as represented by (Swain et al. 2014), who discovered a relation between the rising

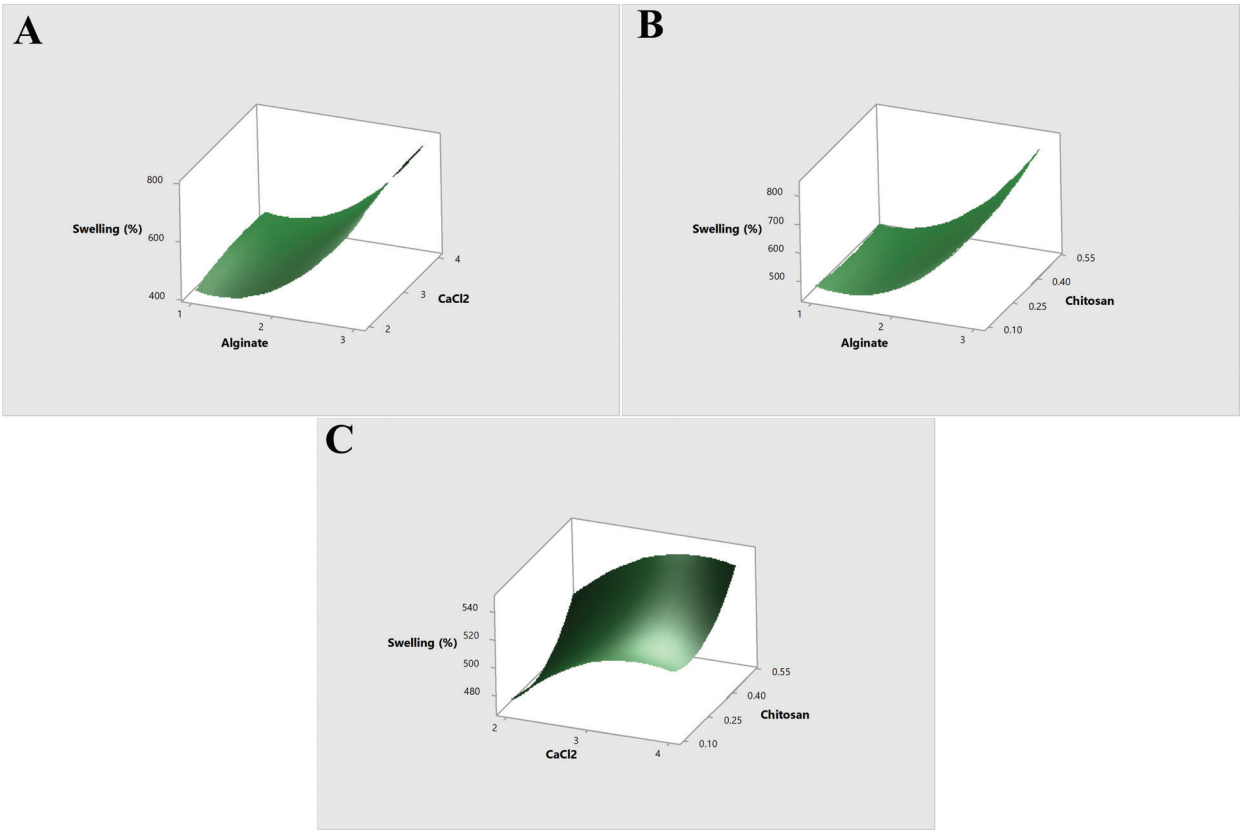

Figure 2. Response surface graphs show variables' effects on (**A, B, C**) swelling%.

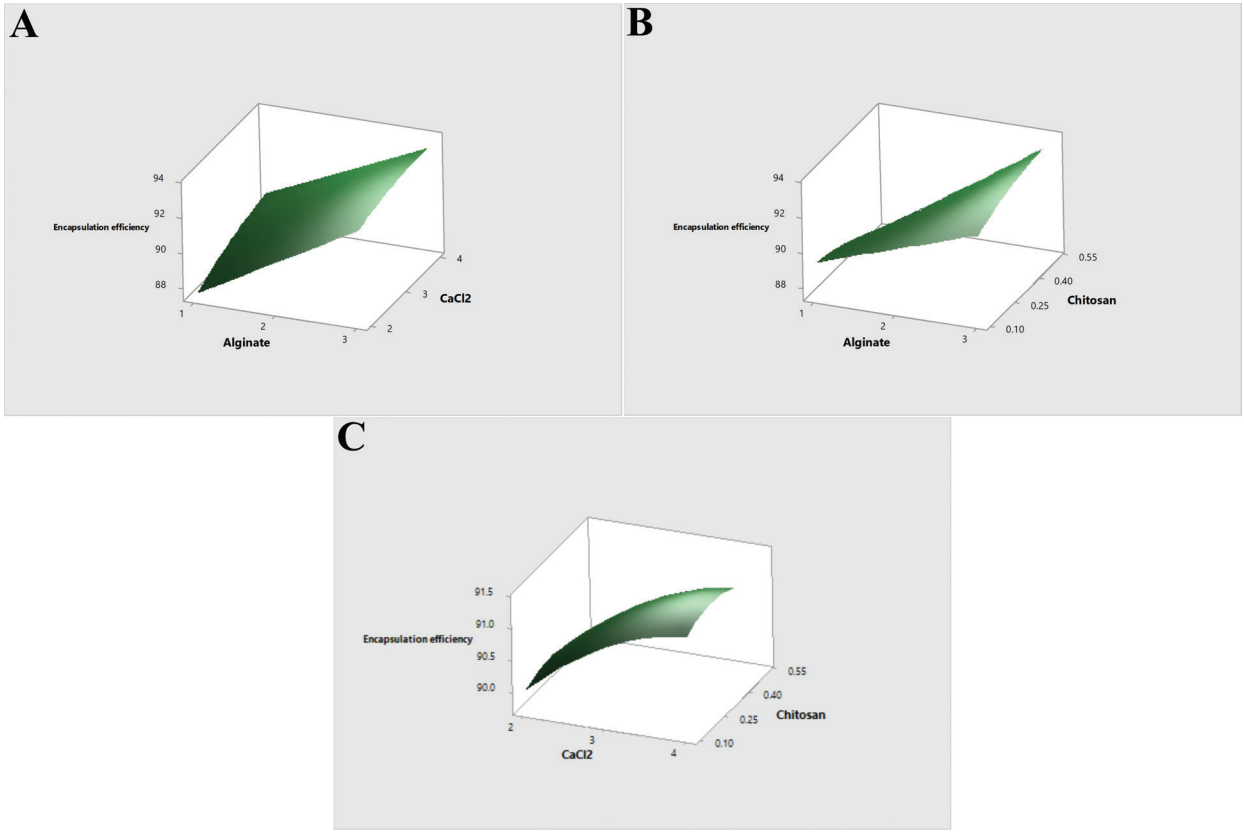

Figure 3. Response surface graphs show variables' effects on (**A, B, C**) encapsulation efficiency (%).

swelling and diameter. Model graphs demonstrated that SAT significantly impacts the EE% of different formulas. Fig. 3A, B show that, as the content of SAT increased, the EE% of different formulae also increased. This is consistent with the results of (Babu et al. 2011), who found the same outcomes: when the SAT was raised, the EE% was significantly raised in different formulas.

Effect of $CaCl_2$

$CaCl_2$ change, when considered in terms of change in SAT, showed no significant effect, which indicates SAT has more effect on the PZ at all concentrations of $CaCl_2$; however, the effect on $CaCl_2$ change when examined against the change in CTN showed variability, in which a larger PS was achieved with low concentrations of $CaCl_2$ and higher concentrations of CTN and the lowest PS was achieved with medium concentrations of $CaCl_2$ and the lowest concentrations of CTN. It is evident from the model graphs displayed in Fig. 1A, C that, with increasing $CaCl_2$ concentration, the response surface shifts from a higher diameter value to a smaller one.

Dissolution of the PZS-HGMG formulated in a low $CaCl_2$ solution occurred sooner than in PZS-HGMG formulated in $CaCl_2$ solutions of higher concentrations, and the maximum SW ratios rose with the increase in $CaCl_2$ concentration at pH 1.2. The concentration of Ca^{2+} during the formulation of PZS-HGMG may improve their cross-linking density. This observation is consistent with those of (Laelorspoen et al. 2014).

It is blatantly obvious in Fig. 1G, I that the EE% was raised when the $CaCl_2$ content was raised due to the cross-linking reaction being favored (Ghumman et al. 2018).

Effect of CTN

As CTN concentration increases, the resulting formulation's diameters rise (Wang et al. 2017). A thicker CTN layer may increase the size of the formulations. This trend lines up with a rise in the mean diameters of the PZS-HGMG, as shown in Fig. 1C.

The SW% index grew dramatically with rising CTN concentrations at pH 1.2. The raised concentration of CTN led to a raised SW% of different formulae (Fig. 2C). This observation is consistent with previous studies (Sinha et al. 2018).

The impacts of CTN concentration on the diameter and EE% of different formulas may explain why a reduction in CTN concentration led to a decline in EE%. The results are shown in Fig. 2C and are consistent with another study (Mi et al. 2013). By elevating the concentration of CTN in the coagulation solution, the density of the resulting membrane is increased as more SAT-CTN ionic interactions are created, resulting in a less perforated gel formation and a higher EE%; this might be because the medicine is less likely to escape from the PZS-HGMG during encapsulation.

Selection of the optimized formula

The optimized formula was chosen by the numerical optimization of Design Expert® software based on the desirability factor's proximity to 1 (Fig. 4). Variable parameters were set in a range. The optimized formula in this experiment would have maximum EE%, SW%, and PZ in the range. The predicted SAT (X1 = 3% w/v), $CaCl_2$

(X2 = 3.818% w/v), and polymer CTN (X3 = 0.5%) were acquired, and this was selected as the optimized formula with a desirability of 0.9814.

These values predict a 2.506 mm diameter, 838.249% SW, and 93.7645% EE. Further characterization confirmed that the optimized formula was valid and determined to be within acceptable ranges.

Morphology of an optimized formula

Fig. 5A shows SEM micrographs of blank HGMC, which were smaller and smoother than the PZS-HGMC optimized formula (Fig. 5B). As can be seen, the surface morphology of drug-loaded MC was regular. The SEM results provided by (Thakral et al. 2010) also displayed similar observations. Fig. 5B shows that the PZS-loaded microcapsules had a spherical appearance.

3.5 FTIR analysis

Infrared spectroscopic analysis for PZS, SAT, CTN, physical mixture HGMC, and the PZS-HGMC optimized formula is shown in Fig. 4. From the data obtained by FTIR (Fig. 6), there are no significant chemical changes between the pure PZS and PZS-HGMC optimized formulas. A stretching endothermic peak marks the characteristic absorption of PZS at 2968.26 cm^{-1}, representing the presence of the C-H group. Another stretching peak appeared at 1647.96 cm^{-1}, which is distinctive to the C = N group. The aromatic ether stretching peak is at 1188.71 cm^{-1}, and the bending peak of the C = C group is displayed at 810.50 cm^{-1}. The FTIR spectrum for the optimized formula exhibited the same peaks as pure PZS at comparable wavelengths, which indicates chemical compatibility between PZS and optimized formula components (Kumar et al. 2016; Nasef et al. 2017).

DSC for optimized formula

The DSC thermograms for PZS, SAT, CTN, the optimized formula physical mixture, and the PZS-HGMC optimized formula are shown in Fig. 6. An endothermic peak at 141.28 °C was observed for pure PZS, corresponding to its melting point. DSC analysis further verifies that the formulation did not involve any drug-polymer interactions. The optimized PZS-HGMG formulation exhibited an endothermic peak at 201.18 °C, characteristic of the polymer matrix. The drug appears to undergo amorphization. The trapping of PZS in the polymer matrix may explain the findings (Abbas and Hanif 2018).

In vitro release and kinetic analysis

Both the free PZS (R^2_{adj} = 0.985) and PZS-HGMC (R^2_{adj} = 0.935) releases followed first-order kinetics (DDSolver 1.0® performed analysis). Fig. 7 shows the cumulative release profile (smother line used). In the case of the free PZS, 95.24±3.2% of PZS was released in the first two hours. This case is unacceptable for drugs that must be sustained and released in the stomach. Fig. 8 shows the drug released from the PZS-HGMC optimized formula in 0.1N HCl (pH = 1.2) fluid. The initial release of drugs from the PZS-HGMG was low. Only 13.21±0.08% of PZS was released after two hours and 40.8±1.2% of PZS after 12 hours; however, after 24 hours, approximately 69.84±2.4% of PZS had been released (Gulia et al. 2023). The film's solidity is compromised by ionization, allowing the PZS to leak out. CTN was dissolved at a pH of 1.2, and after SW and polymer matrix erosion, the PZS was liberated (Sohail et al. 2012).

In vivo treatment efficacy

Evaluation of gastric tissue macroscopic injuries

Macroscopic evaluation of the examined rats' gastric tissues is shown in Fig. 8. The negative control group's gastric tissues (Fig. 9A) exhibited healthy mucosa, minimal redness, and no bleeding or regions of hyperemia. On the other hand, the injured rat groups' (G2 and G3) showed extensive damage to the stomach mucosa (Fig. 9B, C).

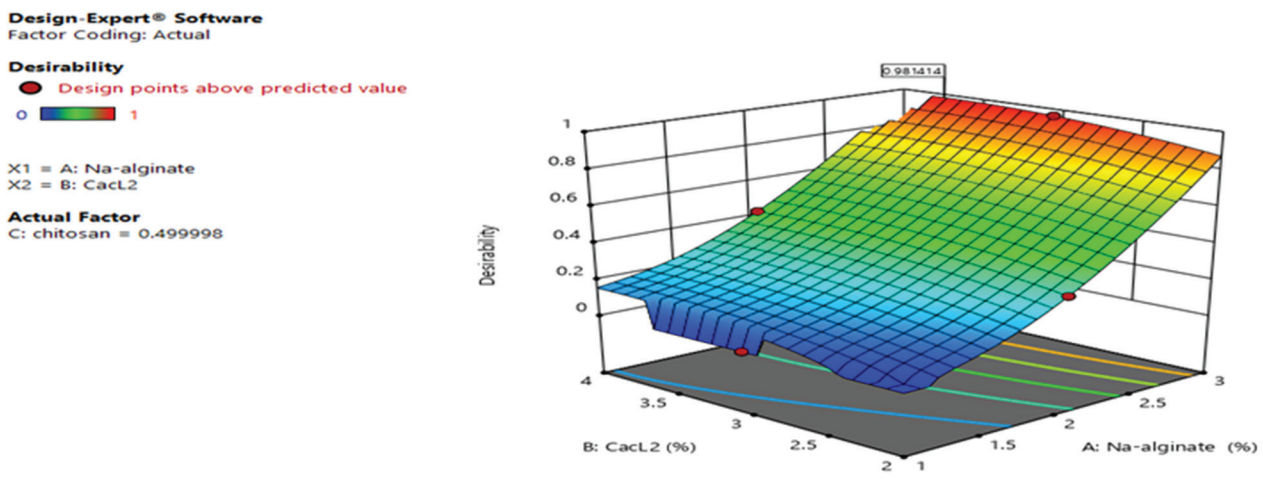

Figure 4. The Design Expert® program forecasted a 3D surface plot displaying the desirability value for optimized formulation.

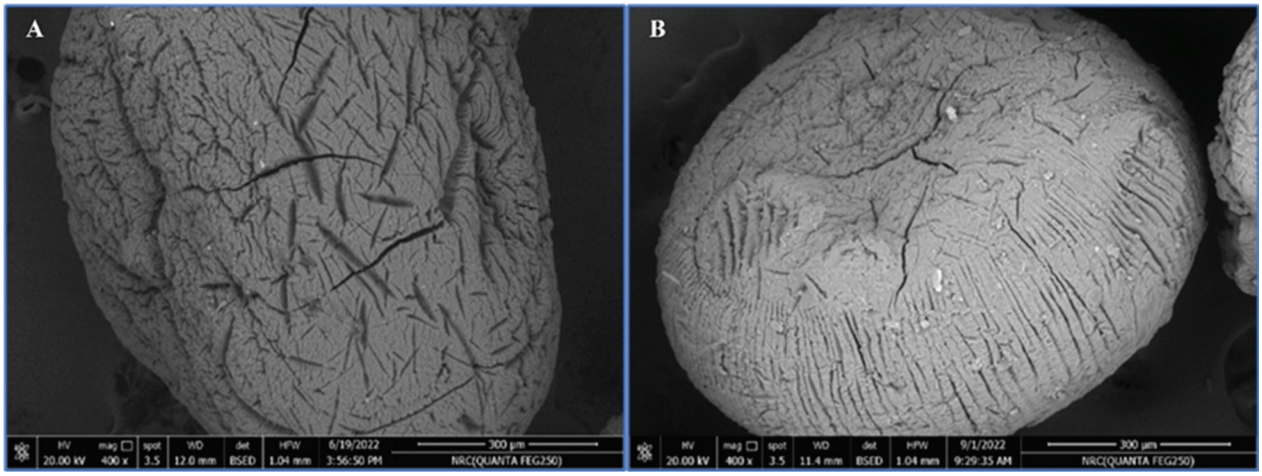

Figure 5. SEM analysis: **A.** Blank (drug-unloaded) HGMC; **B.** PZS-HGM**C.**

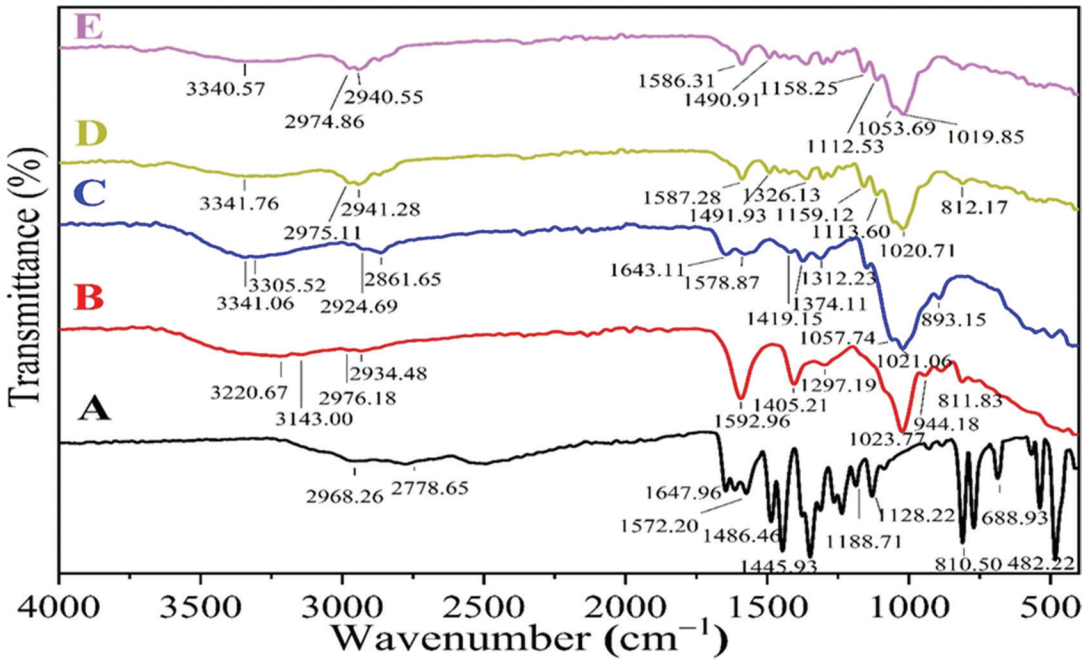

Figure 6. FTIR spectra of **A.** PZS; **B.** SAT; **C.** CTN; **D.** PZS-HGMG physical mixture; **E.** PZS-HGMG formula.

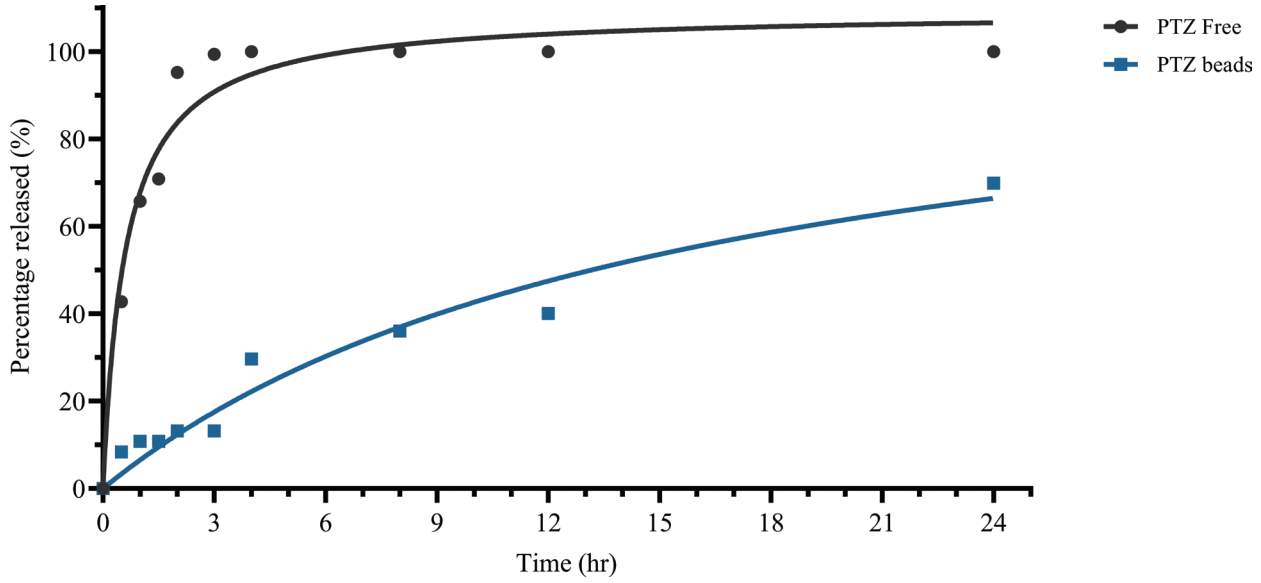

Figure 7. **DSC** spectra of **A.** PZS; **B.** SAT; **C.** CTN; **D.** Optimized formula physical mixture; **E.** Optimized PZS-HGMG formula.

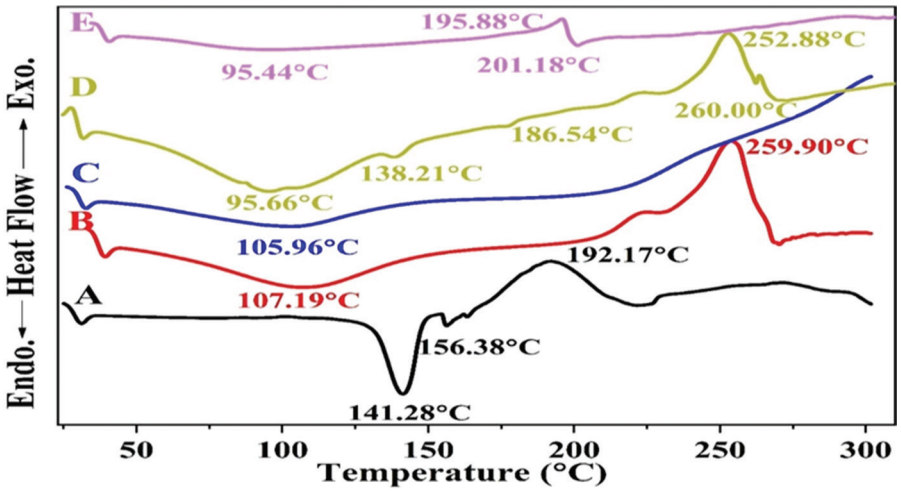

Figure 8. Cumulative drug release (%) of PZS capsule and PZS-HGMC formula in 0.1 N HCl.

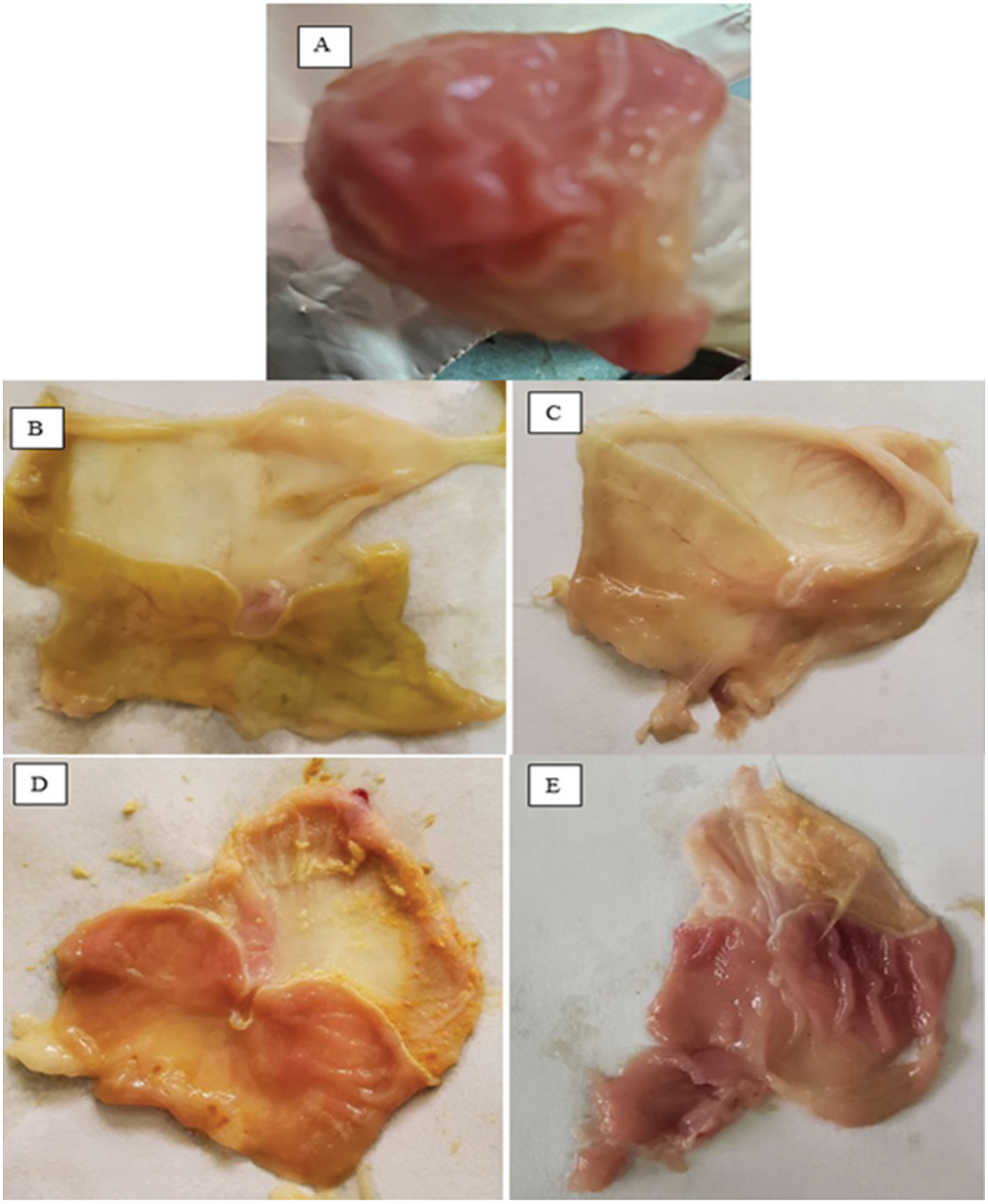

Figure 9. The appearance of the mucosa in the stomachs of IMN-induced rats: **A.** Negative control group; **B.** Positive control group; **C.** Blank MC-treated group; **D.** Free PZS-treated group; **E.** PZS-HGMC-optimized formula-treated group.

When given orally (30 mg/kg), IMN caused severe bleeding sores, most of which were in the gastric glandular mucosa and very few, if any, in the antrum (Yusif et al. 2016). Most of the gastric body was discolored dark reddish from lesions, and the gastric mucosa was riddled with multiple ulcer regions of varying shapes and sizes. The gastric mucosa showed considerable hyperemia.

There were fewer stomach ulcers after administering free PZS to the rats (Fig. 9D). The lesions emerged as discrete lesions in the gastric mucosa, and the epithelial injuries were modest compared to those seen in erythematous control animals (Özgüney 2011). The incision was not observed in any of the medicated rat groups.

On the other hand, medication with a PZS-HGMC optimized formula (Fig. 9E) exhibited an almost typical stomach look, with only a little ulceration and no redness or bleeding.

During the study, the rats in the medicated groups were healthier and behaved normally. The results showed that the medication of animals with PZS-HGMC provided more protection against PUC than medication with free PZS. This could be because the medicine is released slowly over time, retaining a potent concentration of the PZS for a longer period.

Histopathological analysis

The variations in the gastric tissues of the tested rat groups were confirmed through histopathological evaluation. Fig. 10 shows the histopathological analysis of various groups. The gastric histology of the control normal animals (Fig. 10A), which comprise the negative control group (G1), displays a typical glandular structure and function at the microscopic level.

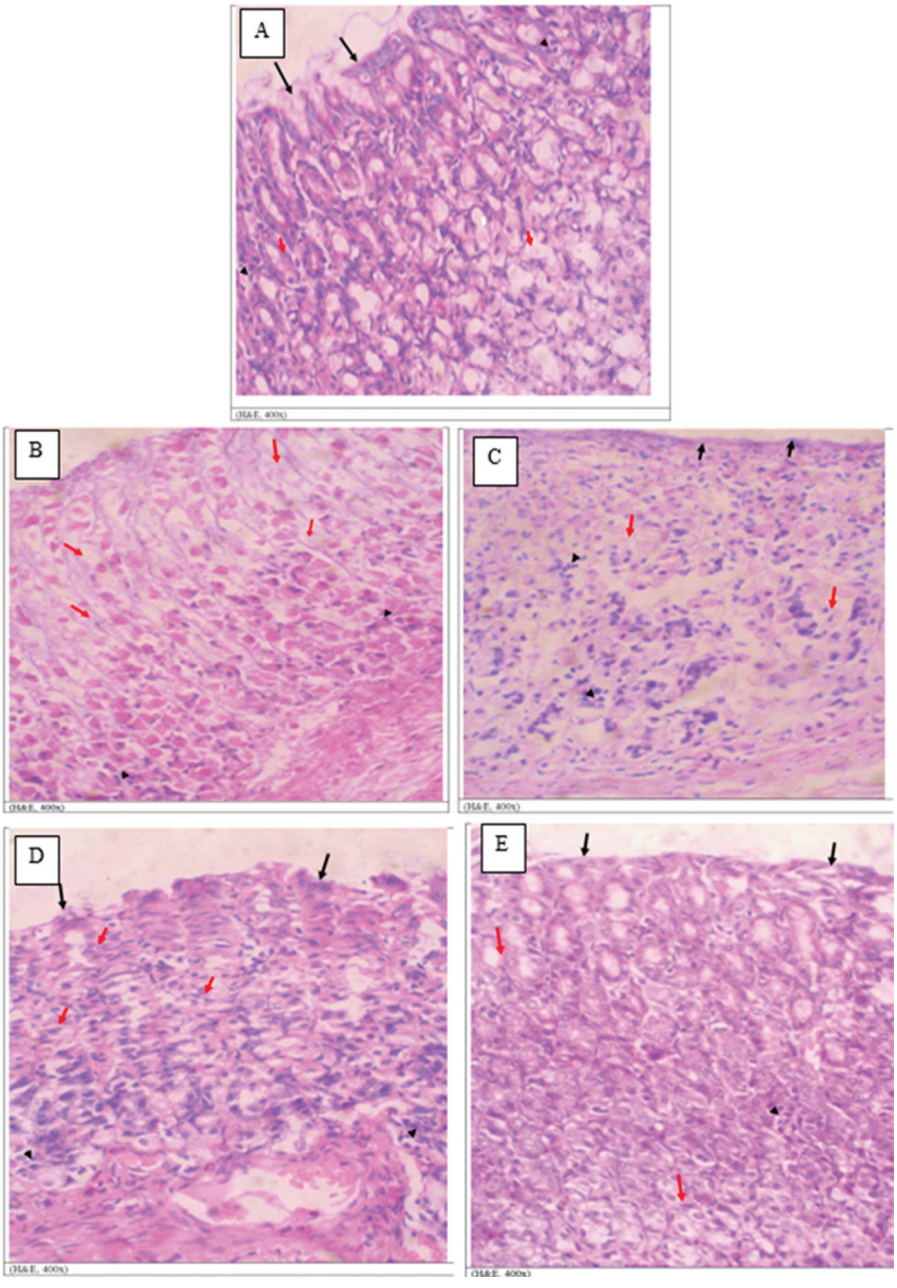

Figure 10. Histological examination of gastric tissues from the INM-induced lesion pattern in rats: **A.** Normal group; **B.** INM-treated control group; **C.** Blank MC-treated group; **D.** Free PZS-treated group; **E.** PZS-HGMC-optimized formula-treated group.

Eccentric nuclei and pale eosinophilic vacuoles in the cytoplasm characterize the parietal cells that make up the top half of the stomach. On the contrary, the IMN-medicated positive control group (G2) (Fig. 10B) shows a prominent inflammatory response characterized by subepithelial edema. The heavily muscled coat was broadened and somewhat hyalinized, and the subepithelial blood arteries were clogged with plaque.

These findings demonstrated the chronic inflammation and acute stage of the lesion. The findings also showed the gastric tissue to be highly inflamed for the INM-medicated group (G3) receiving the blank MC (Fig. 10C). The gastric tissue of (G4), receiving the free PZS, exhibited moderate lesions (Fig. 10D). In (G5), receiving the PZS-HGMC optimized formula (Fig. 10E), the rats had the greatest morphological preservation. They exhibited regular epithelial and lymphatic organization, distribution, and excellent tissue morphology.

Conclusion

In the present study, the oral treatment of IMN-induced PUC in experimental rats with the optimized PZS-HGMC formula for 15 successive days significantly accelerated the recovery of induced PUC compared to the oral treatment with free PZS. SEM photographs showed spherical, smooth surfaces for PZS-HGMG. The FTIR study confirmed the interaction between PZS molecules and the CTN network. DSC showed the dispersion of PZS in the PZS-HGMG network. The effect of different independent variables on diameter, SW%, and EE% was studied for different formulae.

The PZS-HGMC optimized formula has been further examined. The in vitro release of the optimized formula was compared with free PZS in acidic media for 24 hours. The results indicated the release of 95.24±3.2% of free PZS in the first two hours, compared to 13.21±0.08% of the optimized formula. After 24 hours, approximately 69.84±2.4% of PZS was released from the optimized formula. In conclusion, the PZS-HGMC optimized formula exhibited a sustained release effect and improved the healing of PUC compared to free PZS.

Funding

The authors declare that no funds, grants, or other support were received during the preparation of this manuscript.

Competing interests

The authors have no relevant financial or non-financial interests to disclose.

Consent to participate

Not applicable.

References

Abbas G, Hanif M (2018) Development and pharmacokinetic evaluation of alginate-pectin polymeric rafts forming tablets using box behnken design. Drug Development and Industrial Pharmacy 44: 2026–2037. https://doi.org/10.1080/03639045.2018.1508221

Akyuz L, Sargin I, Kaya M, Ceter T, Akata I (2017) A new pollen-derived microcarrier for pantoprazole delivery. Materials Science and Engineering C 71: 937–942. https://doi.org/10.1016/j.msec.2016.11.009

Anal AK, Stevens WF (2005) Chitosan–alginate multilayer beads for controlled release of ampicillin. International Journal of Pharmaceutics 290: 45–54. https://doi.org/10.1016/j.ijpharm.2004.11.015

Babu AK, Teja NB, Ramakrishna B, Kumar B, Reddy GV (2011) Formulation and evaluation of double walled microspheres loaded with pantoprazole. Methods 15: 28.

Bhattacharya S, Chaudhuri SR, Chattopadhyay S, Bandyopadhyay SK (2007) Healing properties of some indian medicinal plants against indomethacin-induced gastric ulceration of rats. Journal of Clinical Biochemistry and Nutrition 41: 106–114. https://doi.org/10.3164/jcbn.2007015

Bigoniya P, Shukla A, Singh CS, Gotiya P (2011) Comparative anti-ulcerogenic study of pantoprazole formulation with and without sodium bicarbonate buffer on pyloric ligated rat. Journal of Pharmacology and Pharmacotherapeutics 2: 179–184. https://doi.org/10.4103/0976-500x.83283

Charan J, Kantharia ND (2013) How to calculate sample size in animal studies? Journal of Pharmacology and Pharmacotherapeutics 4: 303–306. https://doi.org/10.4103/0976-500x.119726

Comoglu T, Gonul N, Dogan A, Basci N (2008) Development and in vitro evaluation of pantoprazole-loaded microspheres. Drug Delivery 15: 295–302. https://doi.org/10.1080/10717540802006864

Dhurke R, Kushwaha I, Desai BG (2013) Improvement in photostability of pantoprazole sodium by microencapsulation. PDA Journal of Pharmaceutical Science and Technology 67: 43–52. https://doi.org/10.5731/pdajpst.2013.00901

Dixon MF, Genta RM, Yardley JH, Correa P, the Participants in the International Workshop on the Histopathology of Gastritis H (1996) Classification and Grading of Gastritis: The Updated Sydney System. The American Journal of Surgical Pathology 20: 1161–1181. https://doi.org/10.1097/00000478-199610000-00001

El-Deen E, El-Mahdy N, Rashidy M, Ghorab M, Gad S, Yassin H (2016) Diclofenac-induced gastric ulceration in rats: Protective roles of pantoprazole and misoprostol. British Journal of Pharmaceutical Research 11: 1–12. https://doi.org/10.9734/BJPR/2016/24636

Elnashar MM, Yassin MA, Abdel Moneim AE-F, Abdel Bary EM (2010) Surprising performance of alginate beads for the release of low-molecular-weight drugs. Journal of Applied Polymer Science 116: 3021–3026. https://doi.org/10.1002/app.31836

Faul F, Erdfelder E, Lang AG, Buchner A (2007) G*Power 3: a flexible statistical power analysis program for the social, behavioral, and biomedical sciences. Behavior Research Methods 39: 175–191. https://doi.org/10.3758/bf03193146

Festing MFW (2006) Design and statistical methods in studies using animal models of development. ILAR Journal 47: 5–14. https://doi.org/10.1093/ilar.47.1.5

Gadge G, Sabale V, Khafe A (2019) Current approaches on gastro retentive drug delivery system: An overview. International Journal of Pharmacy Research & Technology (IJPRT) 9: 16–28. https://doi.org/10.31838/ijprt/09.02.04

Ghumman SA, Bashir S, Noreen S, Khan AM, Riffat S, Abbas M (2018) Polymeric microspheres of okra mucilage and alginate for the controlled release of oxcarbazepine: In vitro & in vivo evaluation. International Journal of Biological Macromolecules 111: 1156–1165. https://doi.org/10.1016/j.ijbiomac.2018.01.058

Gioumouxouzis CI, Chatzitaki A-T, Karavasili C, Katsamenis OL, Tzetzis D, Mystiridou E, Bouropoulos N, Fatouros DG (2018) Controlled Release of 5-Fluorouracil from Alginate Beads Encapsulated in 3D Printed pH-Responsive Solid Dosage Forms. AAPS PharmSciTech 19: 3362–3375. https://doi.org/10.1208/s12249-018-1084-2

Gulia R, Singh S, Arora S, Sharma N (2023) Recent advancements in solubilization and Gastroretentive techniques for Oral Drug Delivery of Proton Pump inhibitors: A comprehensive review. Chemical Biology Letters 10: 546–546.

Gupta NV, Shivakumar HG (2009) Preparation and characterization of superporous hydrogels as pH-sensitive drug delivery system for Pantoprazole sodium. Current Drug Delivery 6: 505–510. https://doi.org/10.2174/156720109789941722

Hamzah ML, Kassab HJ (2024) Formulation and characterization of intranasal drug delivery of frovatriptan-loaded binary ethosomes gel for brain targeting. Nanotechnology, Science and Applications 17: 1–19. https://doi.org/10.2147/NSA.S442951

Han M, Yu Q, Liu X, Hu F, Yuan H (2018) Preparation and characterization of a novel aqueous dispersion for enteric coating of pantoprazole sodium pellets. Acta Pharmaceutica 68: 441–455. https://doi.org/10.2478/acph-2018-0035

Heikal EJ, Kaoud RM, Gad S, Mokhtar HI, Aldahish AA, Alzlaiq WA, Zaitone SA, Moustafa YM, Hammady TM (2023) Design and optimization of omeprazole-curcumin-loaded hydrogel beads coated with chitosan for treating peptic ulcers. Pharmaceuticals 16: 795. https://doi.org/10.3390/ph16060795

Honary S, Maleki M, Karami M (2009) The effect of chitosan molecular weight on the properties of alginate/chitosan microparticles containing prednisolone. Tropical Journal of Pharmaceutical Research 8: 53–61. https://doi.org/10.4314/tjpr.v8i1.14712

Joseph J, Daisy P, George B, Praveenraj R, Thomas N, Betty S (2015) Formulation and evaluation of floating microspheres of Pantoprazole Sodium. International Journal of Pharmacy and Pharmaceutical Research Human 4: 136–147.

Karakas CY, Ordu HR, Bozkurt F, Karadag A (2022) Electrosprayed chitosan-coated alginate–pectin beads as potential system for colon-targeted delivery of ellagic acid. Journal of the Science of Food and Agriculture 102: 965–975. https://doi.org/10.1002/jsfa.11430

Khan MA, Howden CW (2018) The role of proton pump inhibitors in the management of upper gastrointestinal disorders. Gastroenterol Hepatol (N Y) 14: 169.

Khan Z, Abourehab MAS, Parveen N, Kohli K, Kesharwani P (2023) Recent advances in microbeads-based drug delivery system for achieving controlled drug release. Journal of Biomaterials Science, Polymer Edition 34: 541–564. https://doi.org/10.1080/09205063.2022.2127237

Kumar RS, Radha G, Yagnesh TNS (2016) Mucoadhesive microencapsulation: a new tool in drug delivery systems. World Journal of Pharmaceutical Sciences 12: 1410–1470.

Laelorspoen N, Wongsasulak S, Yoovidhya T, Devahastin S (2014) Microencapsulation of Lactobacillus acidophilus in zein–alginate core–shell microcapsules via electrospraying. Journal of Functional Foods 7: 342–349. https://doi.org/10.1016/j.jff.2014.01.026

Lanas A, Chan FKL (2017) Peptic ulcer disease. Lancet 390: 613–624. https://doi.org/10.1016/s0140-6736(16)32404-7

Mi Y, Su R, Fan D-D, Zhu X-L, Zhang W-N (2013) Preparation of N,O-carboxymethyl chitosan coated alginate microcapsules and their application to Bifidobacterium longum BIOMA 5920. Materials Science and Engineering: C 33: 3047–3053. https://doi.org/10.1016/j.msec.2013.03.035

Moghaddam MK, Mortazavi SM, Khayamian T (2015) Preparation of calcium alginate microcapsules containing n-nonadecane by a melt coaxial electrospray method. Journal of Electrostatics 73: 56–64. https://doi.org/10.1016/j.elstat.2014.10.013

Najm WI (2011) Peptic ulcer disease. Prim Care 38: 383–394[, vii]. https://doi.org/10.1016/j.pop.2011.05.001

Nasef AM, Gardouh AR, Ghorab MM (2017) Formulation and in-vitro evaluation of pantoprazole loaded pH-sensitive polymeric nanoparticles. Future Journal of Pharmaceutical Sciences 3: 103–117. https://doi.org/10.1016/j.fjps.2017.04.004

Özgüney Iı (2011) Conventional and Novel Pharmaceutical Dosage Forms on Prevention of Gastric Ulcers. In: Jianyuan C (Ed.) Peptic Ulcer Disease. IntechOpen, Rijeka, Ch. 18. https://doi.org/10.5772/22090

Padhmavathi V, Shruthy R, Preetha R (2023) Chitosan coated skim milk-alginate microspheres for better survival of probiotics during gastrointestinal transit. Journal of Food Science and Technology 60: 889–895. https://doi.org/10.1007/s13197-021-05179-1

Patil P, Chavanke D, Wagh M (2012) A review on ionotropic gelation method: novel approach for controlled gastroretentive gelispheres. International Journal of Pharmacy and Pharmaceutical Sciences 4: 27–32.

Pue MA, Laroche J, Meineke I, de Mey C (1993) Pharmacokinetics of pantoprazole following single intravenous and oral administration to healthy male subjects. European Journal of Clinical Pharmacology - SpringerLink 44: 575–578. https://doi.org/10.1007/bf02440862

Raffin RP, Colomé LM, Schapoval EE, Pohlmann AR, Guterres SS (2008) Increasing sodium pantoprazole photostability by microencapsulation: effect of the polymer and the preparation technique. European Journal of Pharmaceutics and Biopharmaceutics 69: 1014–1018. https://doi.org/10.1016/j.ejpb.2008.01.024

Raj BS, Pancholi J, Samraj PI (2015) Design and evaluation of floating microspheres of pantoprazole sodium. Pharmaceutical and Biosciences Journal 3(6): 09–17. https://doi.org/10.20510/ukjpb/3/i6/87831

Ramos PE, Silva P, Alario MM, Pastrana LM, Teixeira JA, Cerqueira MA, Vicente AA (2018) Effect of alginate molecular weight and M/G ratio in beads properties foreseeing the protection of probiotics. Food Hydrocolloids 77: 8–16. https://doi.org/10.1016/j.foodhyd.2017.08.031

Reddy MS, Jalajakshi B (2018) Formulation and evaluation sustained release mucoadhesive gastroretentive pantoprazole sodium sesquihydrate tablets for anti–ulcer. Journal of Drug Delivery and Therapeutics 8: 304–310. https://doi.org/10.22270/jddt.v8i6-s.2145

Reddy P, Manichandrika KM, Fatima N, Aliya A, Siddiqui K, Begum N (2018) Formulation and evaluation of pantoprazole floating tablets.

International Journal of Advanced Research in Medical & Pharmaceutical Sciences 3: 38. https://doi.org/10.22413/ijarmps/2018/v3/i5/49421

Rostami E (2020) Progresses in targeted drug delivery systems using chitosan nanoparticles in cancer therapy: A mini-review. Journal of Drug Delivery Science and Technology 58: 101813. https://doi.org/10.1016/j.jddst.2020.101813

Sabiu S, Garuba T, Sunmonu T, Ajani E, Sulyman A, Nurain I, Balogun A (2015) Indomethacin-induced gastric ulceration in rats: Protective roles of Spondias mombin and Ficus exasperata. Toxicology Reports 2: 261–267. https://doi.org/10.1016/j.toxrep.2015.01.002

Sheikh A, Asati S (2022) Preparation, evaluation and optimization of solid lipid nanoparticles composed of pantoprazole. Journal of Drug Delivery and Therapeutics 12: 12–18. https://doi.org/10.22270/jddt.v12i1.5154

Shin JM, Sachs G (2008) Pharmacology of proton pump inhibitors. Current gastroenterology reports 10: 528–534. https://doi.org/10.1007/s11894-008-0098-4

Sinha P, Udhumansha U, Rathnam G, Ganesh M, Jang HT (2018) Capecitabine encapsulated chitosan succinate-sodium alginate macromolecular complex beads for colon cancer targeted delivery: in vitro evaluation. International Journal of Biological Macromolecules 117: 840–850. https://doi.org/10.1016/j.ijbiomac.2018.05.181

Sohail A, Bhandari B, Turner MS, Coombes AGA (2012) Direct encapsulation of small molecule hydrophilic and hydrophobic actives in alginate microspheres using a novel impinging aerosols method. Journal of Drug Delivery Science and Technology 22: 139–143. https://doi.org/10.1016/S1773-2247(12)50018-3

Srebro J, Brniak W, Mendyk A (2022) Formulation of dosage forms with proton pump inhibitors: State of the art, challenges and future perspectives. Pharmaceutics 14: https://doi.org/10.3390/pharmaceutics14102043

Sudhakaran N, Koland M, Sindhoor S, Prabhu A (2021) Formulation and evaluation of ion sensitive floating in situ gel of pantoprazole for gastro retentive delivery. Plant Arch 21: 1893–1898. https://doi.org/10.51470/PLANTARCHIVES.2021.v21.S1.307

Swain S, Behera A, Dinda SC, Patra CN, Jammula S, Beg S, Rao ME (2014) Formulation design, optimization and pharmacodynamic evaluation of sustained release mucoadhesive microcapsules of venlafaxine HCl. Indian Journal of Pharmaceutical Sciences 76: 354–363.

Szczepanska M, Sznitowska M (2019) Comparison of the coating process and in vitro dissolution of 3 mm gastro-resistant minitablets and 5 mm gastro-resistant tablets with pantoprazole. Pharmazie 74: 467–470. https://doi.org/10.1691/ph.2019.8180

Taher M, Omer AM, Hamed A, Ali A, Tamer T, Eldin M (2019) Development of smart alginate/chitosan grafted microcapsules for colon site-specific drug delivery. Egyptian Journal of Chemistry 62: 1037–1045. https://doi.org/10.21608/ejchem.2019.6716.1562

Taher YM, Ahmed AA, Fawzi HA, Shalaan N, Alwan AF (2018) Assessment of cardiac function in patients with chronic myeloid leukemia treated with imatinib at the national center of hematology. Asian Journal of Pharmaceutical and Clinical Research 11: 118–120. https://doi.org/10.22159/ajpcr.2018.v11i10.27059

Thakral NK, Ray AR, Majumdar DK (2010) Eudragit S-100 entrapped chitosan microspheres of valdecoxib for colon cancer. Journal of Materials Science: Materials in Medicine 21: 2691–2699. https://doi.org/10.1007/s10856-010-4109-2

Thanos CG, Bintz BE, Bell WJ, Qian H, Schneider PA, MacArthur DH, Emerich DF (2006) Intraperitoneal stability of alginate–polyornithine microcapsules in rats: An FTIR and SEM analysis. Biomaterials 27: 3570–3579. https://doi.org/10.1016/j.biomaterials.2006.01.042

Underwood W, Anthony R (2020) AVMA guidelines for the euthanasia of animals: 2020 edn. [Retrieved on March 2013: 2020–2021]

Wang Y, Zhou J, Guo X, Hu Q, Qin C, Liu H, Dong M, Chen Y (2017) Layer-by-layer assembled biopolymer microcapsule with separate layer cavities generated by gas-liquid microfluidic approach. Materials Science and Engineering: C 81: 13–19. https://doi.org/10.1016/j.msec.2017.07.030

Xie Z, Zhang Y, Xu H, Zhong D (2005) Pharmacokinetic differences between pantoprazole enantiomers in rats. Pharmaceutical Research 22: 1678–1684. https://doi.org/10.1007/s11095-005-6807-x

Yaribeygi H, Hemmati MA, Nasimi F, Maleki M, Jamialahmadi T, Reiner I, Reiner Ž, Sahebkar A (2023) Sodium glucose cotransporter-2 inhibitor empagliflozin increases antioxidative capacity and improves renal function in diabetic rats. Journal of Clinical Medicine 12: 3815. https://doi.org/10.3390/jcm12113815

Yu LY, Sun LN, Zhang XH, Li YQ, Yu L, Yuan ZQ, Meng L, Zhang HW, Wang YQ (2017) A review of the novel application and potential adverse effects of proton pump inhibitors. Advances in Therapy 34: 1070–1086. https://doi.org/10.1007/s12325-017-0532-9

Yuan Y, Padol IT, Hunt RH (2006) Peptic ulcer disease today. Nature Clinical Practice Gastroenterology & Hepatology 3: 80–89. https://doi.org/10.1038/ncpgasthep0393

Yusif RM, Abu Hashim II, Mohamed EA, Badria FA-E (2016) Gastroretentive matrix tablets of boswellia oleogum resin: Preparation, optimization, in vitro evaluation, and cytoprotective effect on indomethacin-induced gastric ulcer in rabbits. AAPS PharmSciTech 17: 328–338. https://doi.org/10.1208/s12249-015-0351-8

Zeeb B, Saberi AH, Weiss J, McClements DJ (2015) Retention and release of oil-in-water emulsions from filled hydrogel beads composed of calcium alginate: impact of emulsifier type and pH. Soft Matter 11: 2228–2236. https://doi.org/10.1039/C4SM02791D